Fundamental and Applied MHD

July 1 – 5, 2019, Reims, France

TURBULENT RAYLEIGH-BENARD CONVECTION IN STRONG VERTICAL MAGNETIC FIELD

R. Akhmedagaev¹, O. Zikanov^{1*}, D. Krasnov², J. Schumacher²

¹ University of Michigan – Dearborn, MI 48128, USA.

*Corresponding author: zikanov@umich.edu

Abstract: Direct numerical simulations are applied to study turbulent Rayleigh-Bénard convection in a vertical cylindrical cavity with uniform axial magnetic field. Flows at moderate Hartmann and Grashof numbers are considered. It is found that the flow is dominated by large-scale coherent structures in the form of near wall jets forming a large-scale circulation roll. Increase of *Ha* from 50 to 100 has an expected effect of suppression on the rate of heat transfer.

Key words: liquid metals, Rayleigh-Bénard magnetoconvection, sidewall modes.

1. Introduction Rayleigh-Bénard convection in the presence of magnetic field has a significant effect on the turbulent transport of heat and momentum in a plethora of natural and industrial processes [2]. Several experiments, most notably [1], indicate that the classical picture of the magnetic field suppressing the flow and, thus, reducing the rate of transport is not always correct. In particular, in systems with sidewalls, a very strong magnetic field may lead to growth of the transport rate and the Nusselt numbers higher than in flows with weak or zero magnetic field at the same Gr. Numerical calculations [3] in a closed square cell revealed the existence and the complex two-layer structure of these modes conducted at a moderate Gr. The goal of our study is to explore the hypothesis that this enhancement is caused by wall modes having the form of ascending/descending jets located near the sidewalls.

2. Presentation of the problem

2.1 Physical model We consider a flow of an incompressible viscous electrically conducting fluid (liquid metal) with constant physical properties contained in a cylinder of the aspect ratio 1 with a uniform axial magnetic field. The top and bottom walls are maintained at constant temperatures. The lateral wall is thermally insulated. All walls are perfectly electrically insulated. Using the Boussinesq and quasi-static approximations we write the non-dimensional governing equations as

$$\nabla \cdot \mathbf{u} = 0 \tag{1}$$

$$\frac{\partial \mathbf{u}}{\partial \mathbf{t}} + (\mathbf{u} \cdot \nabla)\mathbf{u} = -\nabla \mathbf{p} + Re^{-1}\nabla^2 \mathbf{u} + Ha^2 Re^{-1}(\mathbf{j} \times \mathbf{e_z}) + T\mathbf{e_z}$$
 (2)

$$\frac{\partial \mathbf{T}}{\partial \mathbf{t}} + (\mathbf{u} \cdot \nabla)\mathbf{T} = (RePr)^{-1}\nabla^2\mathbf{T}$$
 (3)

$$\mathbf{j} = -\nabla \varphi + \mathbf{u} \times \mathbf{e}_{\mathbf{z}} \tag{4}$$

$$\nabla^2 \varphi = \nabla \cdot (\mathbf{u} \times \mathbf{e}_{\mathbf{z}}) \tag{5}$$

where p, \mathbf{u} , ϕ and T are the fields of pressure, velocity, electric potential, and deviation of temperature from a reference value.

² Ilmenau University of Technology, PO Box 100565 D-98684, Ilmenau, Germany.

The dimensionless control parameters are the Prandtl number, the Reynolds number, the Grashof number or Rayleigh number, the Hartmann number and the aspect ratio:

$$Pr = \frac{v}{\kappa} = 0.025$$
, $Re = \frac{uR}{v} = \sqrt{Gr}$, $Gr = \frac{\beta g \Delta T R^3}{v^2}$, $\Gamma = \frac{H}{D} = 1$.

The Nusselt number is determined at the bottom of the cylinder as

$$Nu = \frac{1}{\pi} \cdot \Gamma^2 \cdot \iint_{bottom} \frac{\partial T}{\partial z} d\Omega$$

and averaged in time over long (not less than 500 units) periods of evolution of fully developed flow.

2.2 Numerical method Governing equations (1) - (5) are solved numerically using the finite difference scheme. The scheme is of the second order and nearly fully conservative in regards of mass, momentum, kinetic energy, and electric charge conservation principles [4, 5]. The time discretization is based on the Adams-Bashforth/Backward-Differentiation method of the second order. At every time step, the three elliptic equations – the projection method equation for pressure, the equation for temperature (3) and for potential (5) are solved using the FFT transform in the azimuthal direction and the cyclic reduction direct solver in the r-z- plane. The computational grid is clustered toward the wall according to the coordinate transformation:

$$z = \frac{\tanh(A_z\zeta)}{\tanh(A_z)}, \qquad r = 0.9\sin(\eta \pi/2) + 0.1\eta$$

where $-1 \le \zeta \le 1, 0 \le \eta \le 1$ are the coordinates, in which the grid is uniform. More details of the numerical method are described in [5, 6].

- 2.3 Grid sensitivity study The flow regimes have been calculated for Ha = 50, 100 and $Gr = 10^6 10^8$. A grid sensitivity study was performed to analyze the minimum requirements for accurate modelling of the flow. We have found that at Ha = 50 the grid with 64, 100 and 48 points in the azimuthal, axial and radial directions, respectively, and $A_z = 2.0$ is sufficient. The grid has 9 points in the Hartmann layer and stable at $\Delta t = 10^{-3}$. Further refinement of the grid changes Nu by less than 1%. The same analysis accomplished for Ha = 100 shows that the grid with 64, 128 and 64 points and with $A_z = 2.5$ is sufficient. This grid has 11 points in the Hartmann layer and stable at $\Delta t = 5 \times 10^{-4}$.
- 3. **Results** The simulations have been performed for Ha = 50, 100 and the ratio $Gr/Gr_c = 10 100$ (table 1) where the critical Grashof number for a horizontally infinite layer [7] is $Gr_c = \frac{\pi^2 Ha^2}{Pr}$.

We see in Table 1 and Fig. 1 that Nu = 1 at $Gr = Gr_c(Ha)$. Analysis of the computed solutions confirms that there is no convection flow in these states. We should note that significant flow dominated by wall modes was detected in [3] at $Gr \leq Gr_c$, but at much higher Ha and Gr.

Another aspect of the results is that increase of Ha from 50 to 100 at the same Gr suppresses convection (see Fig. 1a). At the same time, at equal values of Gr/Gr_c , the flows at Ha = 100 have substantially higher Nu (see Fig. 1b).

Gr/Gr _c	На	Gr	Nu	На	Gr	Nu
1		9.86×10^{5}	1.00		3.94×10^{6}	1.00
10		9.86×10^{6}	3.70		3.94×10^{7}	4.70
20		1.97×10^{7}	4.46		7.89×10^{7}	6.18
30		2.96×10^{7}	4.99		1.18×10^{8}	7.04
40	50	3.94×10^{7}	5.36	100	1.58×10^{8}	7.64
50		4.93×10^{7}	5.66		1.97×10^{8}	8.21
60		5.92×10^{7}	5.91		2.37×10^{8}	8.52
70		6.90×10^{7}	6.25		2.76×10^{8}	9.11
80		7.89×10^{7}	6.34		3.16×10^{8}	9.49
90		8.87×10^{7}	6.67		3.55×10^{8}	9.94
100		9.86×10^{7}	6.79		3.94×10^{8}	9.92

Table 1: Summary of the simulation results.

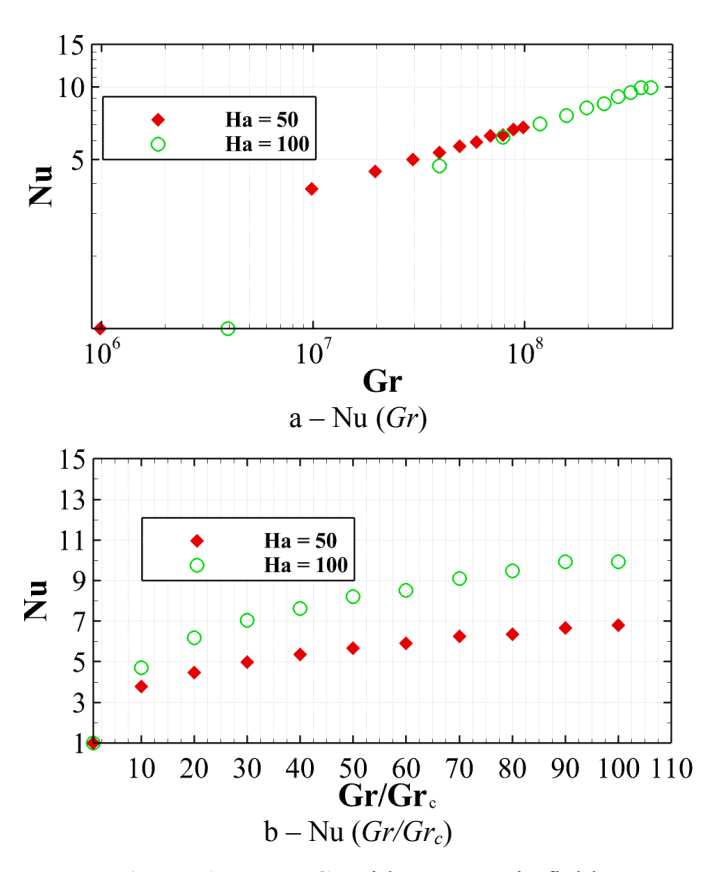


Figure 1: Nu vs Gr with a magnetic field.

Fig. 2 displays snapshots of the temperature and velocity fields. The flow has a cellular form with ascending and descending jets filling the entire cylinder at Ha = 50. At Ha = 100 these structures tend to be nearer to the vertical wall. Flows at $Gr/Gr_c = 10$ are unsteady with a regular structure. At $Gr/Gr_c = 100$, the flows are less regular, but retain the large-scale pattern.

To analyze the evolution of the large-scale circulation pattern with time, we have recorded the location of the temperature maximum on the equatorial line of the side wall z=0, r=1. This location approximately corresponds to the center of the ascending near-wall jet. The typical results are illustrated in Fig. 3. We see that the plane of the large-scale circulation fluctuates quasi-periodically in φ around a constant and slowly shifting mean. The characteristics of the process are strongly affected by Ha and Gr.

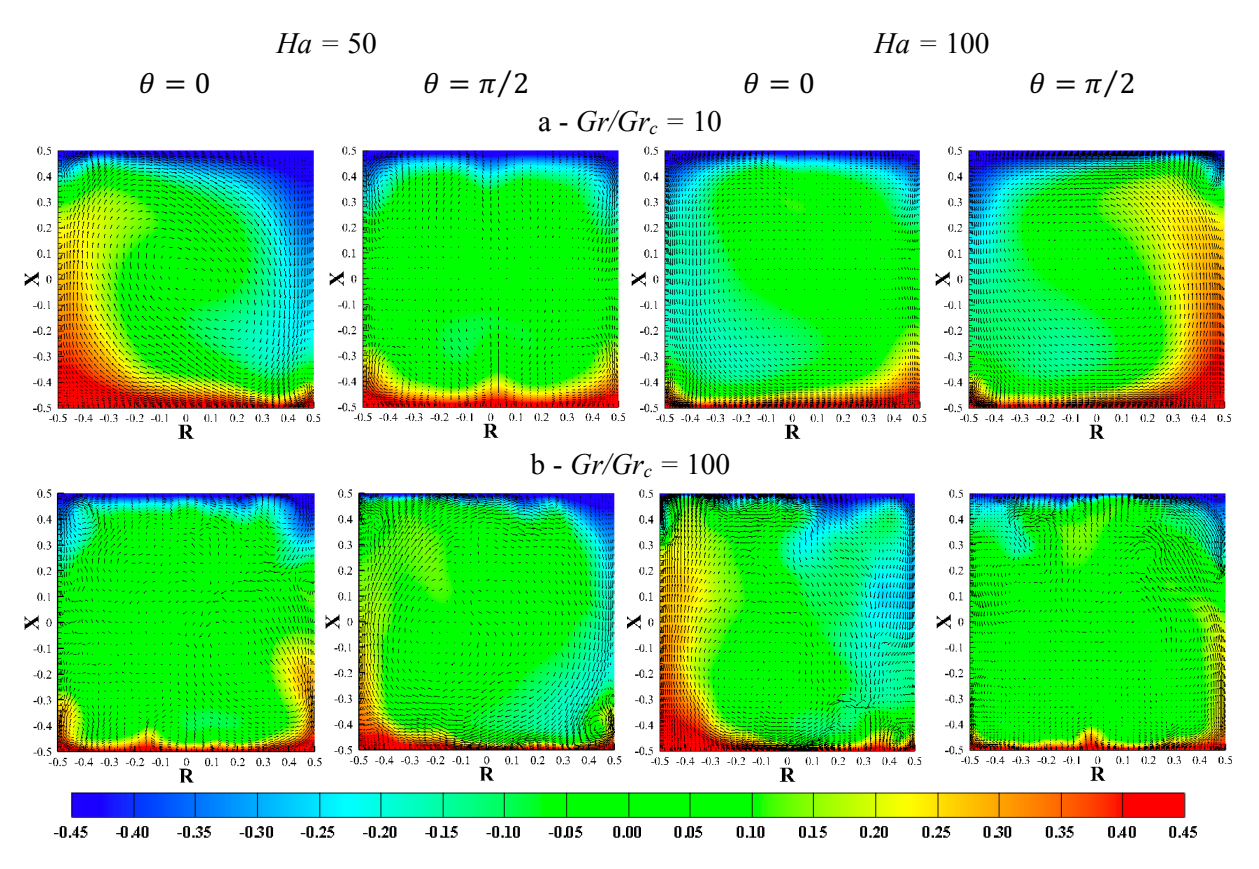


Figure 2: Flow structure at Ha = 50 (left) and Ha = 100 (right) and $Gr/Gr_c = 10$ (top) and $Gr/Gr_c = 100$ (bottom). Instantaneous distributions of temperature and vectors of velocity are shown in the vertical cross-sections through the axis of the cylinder.

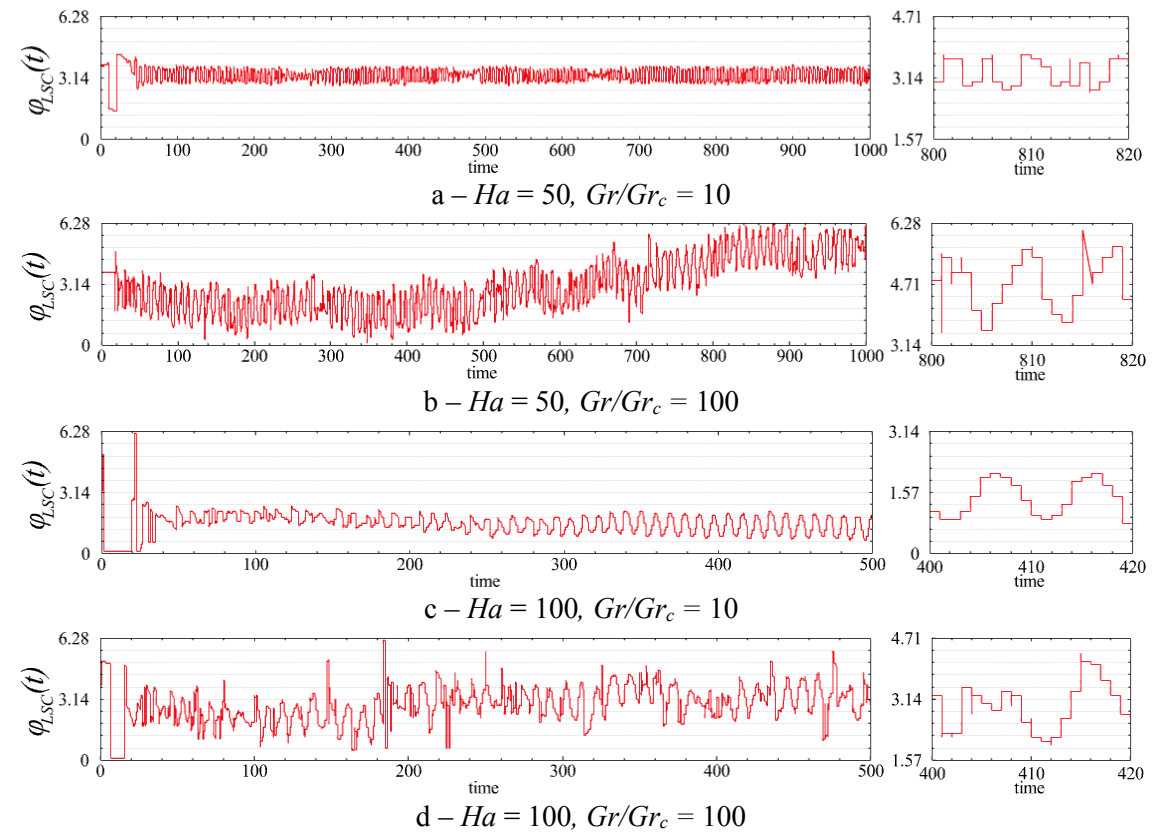


Figure 3: Time history of the location of the maximum temperature at z = 0, r = 1.

11th PAMIR International Conference - Fundamental and Applied MHD July 1 – 5, 2019, Reims, France

4. Conclusions We have analyzed the Rayleigh-Bénard convection in a cylinder at Ha = 50, 100 and $Gr = 10^6 - 10^8$. The flows are dominated by the large-scale fluctuating but otherwise robust circulation rolls. The magnetic field reduces the heat transfer. Further simulations at higher Ha and Gr are planned for the future.

Acknowledgments Financial support is provided by the US NSF (Grant CBET 1803730) and by the DFG (Grant KR 4445/2-1).

REFERENCES

- [1] S. CIONI, S. CHAUMAT, J. SOMMERIA. Effect of a vertical magnetic field on turbulent Rayleigh-Bénard convection. *Physical Review E*, 62(4), R4520, 2000.
- [2] P. A. DAVIDSON. Introduction to Magnetohydrodynamics. Cambridge University Press, 2016.
- [3] W. LIU, D. KRASNOV, J. SCHUMACHER. Wall modes in magnetoconvection at high Hartmann numbers. *J. Fluid Mech.*, vol. 849, R2, 2018.
- [4] M. J. NI, R. MUNIPALLI, N. B. MORLEY, P. HUANG, M. A. ABDOU. A current density conservative scheme for incompressible MHD flows at a low magnetic Reynolds number. Part I: On a rectangular collocated grid system. *J. Comp. Physics*, vol. 227, 2007.
- [5] D. KRASNOV, O. ZIKANOV, T. BOECK. Comparative study of finite difference approaches in simulation of magnetohydrodynamic turbulence at low magnetic Reynolds number. *Comp. Fluids*, vol. 50, 2011.
- [6] O. ZIKANOV, Y. I. LISTRATOV, V. G. SVIRIDOV. Natural convection in horizontal pipe flow with a strong transverse magnetic field. *J. Fluid Mech.*, vol. 720, 2013.
- [7] S. CHANDRASEKHAR. Hydrodynamic and Hydromagnetic Stability. Dover, 1961.